Does global warming cause intensified interannual hydroclimate variability?

Richard Seager * and Naomi Naik

Lamont Doherty Earth Observatory of Columbia University, Palisades, New York†

Laura Vogel

Columbia College, New York, New York

* *Corresponding author address:* Richard Seager, Lamont Doherty Earth Observatory of Columbia University, 61 Route 9W., Palisades, NY 10964.

E-mail: seager@ldeo.columbia.edu

† LDEO Contribution number xxxx

ABSTRACT

The idea that global warming leads to more droughts and floods has become commonplace without clear indication of what is meant by this statement. Here we examine one aspect of this problem and assess whether interannual variability of precipitation (P) minus evaporation (E) becomes stronger in the 21^{st} Century compared to the 20^{th} Century, as deduced from an ensemble of models participating in Coupled Model Intercomparison Project 3. It is shown that indeed interannual variability of $P - E$ does increase almost everywhere across the planet with a few notable exceptions such as southwestern North America and some subtropical regions. The variability increases most at the Equator and the high latitudes and least in the subtropics. While most interannual $P - E$ variability arises from internal atmosphere variability the primary potentially predictable component is related to the El Niño-Southern Oscillation (ENSO). ENSO-driven interannual $P - E$ variability clearly increases in amplitude in the tropical Pacific but elsewhere the changes are more complex. This is not surprising in that ENSO-driven $P - E$ anomalies are primarily caused by circulation anomalies combining with the climatological humidity field. As climate warms and the specific humidity increases this term leads to an intensification of ENSO-driven $P - E$ variability. However, ENSO-driven circulation anomalies also change, in some regions amplifying, but in others opposing and even overwhelming, the impact of rising specific humidity. Consequently there is sound scientific basis for anticipating a general increase in interannual $P - E$ variability but the predictable component will depend in a more complex way on both thermodynamic responses to global warming and on how tropically-forced circulation anomalies alter.

1. Introduction

According to projections with climate models global warming driven by rising greenhouse gas concentrations will cause significant changes in the distribution of precipitation (P) minus evaporation (E) at the Earth's surface. These can be summarized as dry areas getting drier and wet areas getting wetter and a poleward and equatorward expansion of the subtropical dry zones. These changes arise from intensified atmospheric moisture transports in a warmer, more moist, atmosphere and a poleward expansion of Hadley Cell, poleward shift of the mid-latitude storm tracks and equatorward contraction of convergence zones (Held and Soden 2006; Seager et al. 2007; Intergovernmental Panel on Climate Change 2007; Neelin et al. 2006; Chou et al. 2009; Seager et al. 2010c). These changes in $P - E$ will create problems in water-stressed arid zones as well as add to flooding hazards in regions expected to get wetter. However, natural climate variability on day-to-day, month-to-month, year-to-year and decade-to-decade timescales already causes havoc in terms of agricultural losses, transportation disruption by storms, shortfalls in municipal water supply, flooding in low-lying areas, death by starvation following disrupted food availability or in heat waves and so on. Recent examples of disruption, suffering and death caused by climate events that, if not entirely unsullied by the influence of anthropogenic climate change contain a large component of natural climate variability, are the intensely cold and snowy 2009/10 winter in the eastern U.S. and northwest Europe (Seager et al. 2010b; Cattiaux et al. 2010), the Pakistan floods (Webster et al. 2011) and Russian heat wave (Dole et al. 2011) of summer 2010, the intense flooding in northeast Australia early in 2011 and the China drought of winter 2010/11. While it is clearly important to develop means to adapt to long term climate trends a strong case can be made that developing resilience to the worst challenges that natural climate variability can pose will, in and of itself, create a basic level of resilience to anthropogenic climate change (Sarachik 2011). Indeed, for countries such as Pakistan, where whole communities were washed away in the 2010 monsoon floods, it makes little sense to adapt to a multidecadal timescale trend when the countries' infrastructure is so severely stressed by already-existing (dominantly natural) year-to-year variability.

As Sarachik (2011) says 'mitigation is about climate trends, adaptation is about climate variability'. But this does not let climate change off the hook in terms of adaptation. There is a growing sense that a purely 'natural', i.e. uninfluenced by human activity, climate system no longer exists and it is widely assumed that climate events like heat waves, stormy winters, droughts and floods, bear at least some imprint of human-induced climate change rendering the term 'natural climate variability' a relic of the pre-industrial age. It is commonly stated, for example, that global warming will simultaneously lead to more floods and droughts and more climate extremes. As a fairly typical example of common assumptions, writing in the *New York Times* on August 15 2010, Justin Giles stated 'Theory suggests that a world warming up ..... will feature heavier rainstorms in summer, bigger snowstorms in winter, more intense droughts in at least some places and more record-breaking heat waves'. That is, global warming will lead to more extreme climate variability on all timescales.

Increases in atmospheric humidity associated with warming provide a rationale for these assumptions: any given circulation anomaly can draw on more moisture than before and create more precipitation. This argument is used to explain observed increases in the proportion of total precipitation falling in the most intense events (Trenberth et al. 2003; Groisman et al. 2005) although to our knowledge proof of this assertion has not yet been forthcoming. However, if this is so on short timescales of days or less, the same process should work on interannual timescales. For example ENSO-related $P-E$ anomalies and tropical Pacific forced decadal precipitation changes are fundamentally driven by changes in circulation acting on the climatological humidity field (Huang et al. (2005); Seager (2007); Seager and Naik (2011) and below). As specific humidity rises these same forced circulation anomalies should cause more intensified $P-E$ variability and, hence, more extreme droughts and floods.

But does interannual $P-E$ variability intensify as climate warms? Given that interannual $P-E$ variability is forced by circulation anomalies it is possible that changes in SST variability or atmosphere dynamics could also create changes in $P-E$ variability that offset, or maybe amplify, the expected increase due to thermodynamic processes alone. While adaptation to climate variability is a good first step towards adaptation to climate change it needs to be known what climate variability to adapt to. Most countries in the world are already stressed by climate variability (including wealthy ones with well developed infrastructure as evidenced by, for example, drought in the southeast U.S. in 2006/7 (Seager 2007) and floods in the U.K. in 2000 (Pall et al. 2011)) and if global warming causes the variability to get more extreme this needs to be known. That is what we examine here focusing on the year-to-year timescale. On this timescale the dominant mode of global $P-E$ variability is the El Niño-Southern Oscillation (ENSO). We will examine the Coupled Model Intercomparison Project 3 (CMIP3) archive used by the Intergovernmental Panel on Climate Change (IPCC) Assessment Report 4 (AR4) (Meehl et al. 2007) using simulations of the 20th Century and projections of the current century in all the models that make all the needed data available. We will look at how ENSO-related $P-E$ variability changes and separate this into changes in the dynamic (caused by circulation anomalies) and thermodynamic (caused by humidity anomalies) components and then look at how these contributions change between the centuries and, to the extent we can, why.

Increased amplitude of interannual variability as a consequence of global warming would create new problems for societies struggling to adapt to already-existing interannual variability. This would be in addition to any additional challenges posed by trends in the mean climate state. As we will show model projections of current century climate show a widespread but not universal increase in the amplitude of the total interannual variability of $P-E$ and of the ENSO-driven component in many places. However, in some regions changes in circulation variability offset changes due to increasing humidity leading to little change in, or even reduced, amplitude of $P-E$ variability.

2. Model data used and methodology

We analyze 15 models from the CMIP3/IPCC AR4 archive. The models were selected because all of the needed data were available and free of errors. We analyze both the 20^{th} Century simulations with known and estimated past climate forcings and the projections of 21^{st} Century climate using the 'middle-of-the-road' SResA1B emissions scenario. In prior work (Seager et al. 2010a; Seager and Naik 2011) we have analyzed only those models and time periods for which all the daily data needed to evaluate transient eddy moisture convergences were available (1961-2000 and 2046-65). Seager and Naik (2011) showed that

ENSO-forced $P-E$ variability is dominated in these CMIP3/IPCC AR4 models by changes in the mean circulation combining with the climatological moisture field to create anomalous convergence and divergence of moisture. They found that contributions from both variability in humidity and changes in moisture convergence or divergence by transient eddies (defined as co-variances of submonthly wind and specific humidity fields) were decidedly of secondary importance. Here we do not seek to evaluate changes in the variability of transient eddy moisture convergence and divergence. Instead we choose to improve the characterization of contributions to $P-E$ variability from changes in mean quantities by using the entire centuries of modeled data.

We begin with the vertically integrated moisture budget equation which balances $P-E$ with convergence of moisture by the mean and transient flow,viz:

$$\rho_w g(\overline{P}-\overline{E}) \approx -\int_0^{\overline{p}_s} \left(\nabla \cdot (\overline{\overline{\mathbf{u}}}\,\overline{\overline{q}} + \overline{\overline{\mathbf{u}}}\hat{q} + \hat{\mathbf{u}}\overline{\overline{q}}\right) dp - \int_0^{\overline{p}_s} \nabla \cdot (\overline{\mathbf{u}'q'})dp - \overline{q_s\mathbf{u}_s \cdot \nabla p_s}, \qquad (1)$$

In Equation 1 the climatological monthly mean quantities are represented by double overbars, monthly means by single overbars, monthly departures from the climatological monthly mean by hats and departures from monthly means by primes. Total fields are given by, for example, $\mathbf{u} = \overline{\mathbf{u}} + \mathbf{u}' = \overline{\overline{\mathbf{u}}} + \hat{\mathbf{u}} + \mathbf{u}'$. Products of monthly anomalies have been neglected. ρ_w is water density, g is the acceleration due to gravity, p is pressure, p_s surface pressure, $\mathbf{u}$ is the horizontal vector wind and $\mathbf{u_s}$ its surface value and q is specific humidity. The first term on the right hand side is the moisture convergence by the mean flow and the second term the moisture convergence by the submonthly transient eddies. (The third term provides a general tendency to reduce $P-E$ (because of surface flow down the pressure gradient) but cannot be evaluated for all models since many did not save daily values of surface winds and humidity. Within the GFDL CM2.1 model this term was evaluated with daily data and then found to be reasonably approximated using monthly data. We then evaluated it for all models using monthly data. It is several times smaller than the other two terms and we discuss it no more.)

The dominant mode by far of global $P-E$ variability is ENSO. Hence we will focus on potential changes in the interannual variability of ENSO-forced $P-E$ variability. We break down the moisture budget into a term related to variability in circulation and a term related to variability in humidity, variability in transient eddy moisture convergence and variability in the boundary term. Introducing the notation:

$$\langle \mathbf{A} \rangle^T = \int_0^{\overline{p}_s, T} (\nabla \cdot \mathbf{A}) dp. \tag{2}$$

The superscript T indicates the time period, i.e. 20^{th} or 21^{st} Century, corresponding to the pressure data for the vertical integral. Below the subscript T indicates a time period for the subscripted variable. Then we have for the case of ENSO variability:

$$\rho_w g \delta(\bar{P} - \bar{E}) \approx \delta TH + \delta MCD + \delta TE - \delta S, \tag{3}$$

$$\delta TH = -\delta \langle \overline{\overline{\mathbf{u}}}_T \hat{q}_T \rangle^T, \tag{4}$$

$$\delta MCD = -\delta \langle \hat{\mathbf{u}}_T \overline{\overline{q}}_T \rangle^T, \tag{5}$$

$$\delta TE = -\delta \langle (\overline{\mathbf{u}' q'})_T \rangle^T, \tag{6}$$

$$\delta S = \delta (\overline{q_s \mathbf{u}_s \cdot \nabla p_s})_T. \tag{7}$$

The term influenced only by changes in humidity is called the thermodynamic term, δTH and the term influenced only by changes in the mean circulation is called the dynamic term, δMCD. δTE is the term related to changes in transient eddy fluxes and δS is the change in the boundary term. The difference δ, is given by:

$$\delta(\cdot) = [\cdot]_{LN} - [\cdot]_{EN}, \tag{8}$$

where the square brackets with subscripts LN and EN indicate time-averaging over months with La Niña or El Niño conditions of the quantity in parentheses. The approximate equality in Eq. 3 assumes that the vertically integrated climatological term is the same averaged over El Niño events as over La Niña events despite the differing limits on the pressure integral i.e. $\left[\langle \bar{\bar{\mathbf{u}}}_T \overline{\overline{q}}_T \rangle^T\right]_{EN} \approx \left[\langle \bar{\bar{\mathbf{u}}}_T \overline{\overline{q}}_T \rangle^T\right]_{LN}$.

El Niño and La Niña conditions are found by conducting an Empirical Orthogonal Function (EOF) analysis of the annual mean $P-E$ field in each model and for each century, after detrending to remove the century-long trends. In all models the first EOF is the model's representation of ENSO explaining between 15 to 49% of the total variance of $P-E$ with a mean of 32%, comparable to that observed (see SN). To compute La Niña minus El Niño differences we take the associated principal component for each model and compute composites over all years when it exceeds one standard deviation and all years over which it is below one standard deviation. This difference is the La Niña minus El Niño composite difference. Here we only show the multimodel ensemble mean (MEM) of the composite differences.

To analyze the change in the $P-E$ variability we will need to determine what causes 20^{th} to 21^{st} Century changes in the MCD and TH contributions, i.e. how changes in the mean and variability of specific humidity and circulation cause changes in the dynamic and thermodynamic drivers of $P-E$ variability. To do this we define a 21^{st} Century minus 20^{th} Century change as:

$$\Delta(\cdot) = (\cdot)_{21} - (\cdot)_{20}, \tag{9}$$

where the subscripts 21 and 20 refer to 21^{st} and 20^{th} Century averages. Hence $\bar{\mathbf{u}}_{21} = \bar{\mathbf{u}}_{20} + \Delta\bar{\mathbf{u}}$, $\delta\bar{q}_{21} = \delta\bar{q}_{20} + \Delta\delta\bar{q}$, etc. Hence the change in $P-E$ variability can be divided up into changes in the variabilities of the thermodynamic term, the mean circulation dynamics term and the transient eddy and boundary terms, viz:

$$\rho_w g \Delta\left(\delta(P-E)\right) \approx \Delta\left(\delta TH\right) + \Delta\left(\delta MCD\right) + \Delta\left(\delta TE\right) - \Delta\left(\delta S\right). \tag{10}$$

Substituting the relations for 21^{st} and 20^{th} Century values into Equation 3, and neglecting terms nonlinear in Δ (such as $\Delta\bar{\mathbf{u}}\Delta\bar{q}$), gives:

$$\Delta\left(\delta TH\right) \approx \Delta\left(\delta TH_q\right) + \Delta\left(\delta TH_u\right), \tag{11}$$

$$\Delta\left(\delta TH_q\right) = -\delta\langle\bar{\bar{\mathbf{u}}}_{20}\Delta\hat{q}\rangle^{21}, \tag{12}$$

$$\Delta\left(\delta TH_u\right) = -\delta\langle\Delta\bar{\bar{\mathbf{u}}}\,\hat{q}_{20}\rangle^{21}, \tag{13}$$

that is, the change in the thermodynamic contribution to $P-E$ variability involves a term (Eq. 11) that is caused by a change in the humidity variability combining with the unchanged circulation and a term (Eq. 12) that is caused by a change in the mean circulation combining with the unchanged humidity variability. The approximation in Eq. 10 assumes that $\delta\langle\bar{\bar{\mathbf{u}}}_{20}\hat{q}_{20}\rangle^{21} \approx \delta\langle\bar{\bar{\mathbf{u}}}_{20}\hat{q}_{20}\rangle^{20}$ which was assessed and found to be valid.

Similarly the mean circulation dynamics contribution to the change in $P-E$ variability breaks down as:

$$\Delta\left(\delta MCD\right) \approx \Delta\left(\delta MCD_q\right) + \Delta\left(\delta MCD_u\right), \tag{14}$$

$$\Delta\left(MCD_q\right) = -\delta\langle \hat{\mathbf{u}}_{20} \Delta \overline{\overline{q}} \rangle^{21}, \tag{15}$$

$$\Delta\left(MCD_u\right) = -\delta\langle \Delta\hat{\mathbf{u}}\, \overline{\overline{q}}_{20} \rangle^{21}, \tag{16}$$

that is, a term (Eq. 14) caused by the change in mean humidity combining with the unchanged circulation variability and a term (Eq. 15) caused by a change in the circulation variability combining with the unchanged humidity. The approximation in Eq. 13 assumes that $\delta\langle \hat{\mathbf{u}}_{20} \overline{\overline{q}}_{20} \rangle^{21} \approx \delta\langle \hat{\mathbf{u}}_{20} \overline{\overline{q}}_{20} \rangle^{20}$ which was also assessed and found to be valid.

At this point it should be noticed that the breakdown of $P-E$ variability into thermodynamic and dynamic contributions is no longer absolute. As climate changes and climatological mean specific humidity and circulation change the efficiency of the thermodynamic and dynamic contributions to $P-E$ variability will change. For example $P-E$ variability that arises from specific humidity variability will differ as the climatological mean circulation that converges the humidity anomalies alters. Similarly the increase in climatological mean specific humidity accompanying global warming appears in the $\Delta\left(MCD_q\right)$ term where it acts to make the circulation variability more effective: i.e. the same amplitude of circulation variability in the 21^{st} Century as in the 20^{th} Century creates a tendency to larger $P-E$ variability because it is operating on a enhanced mean moisture field.

3. Changes in model simulated total interannual $P-E$ variability

While the remainder of the paper considers changes in $P-E$ variability associated with the leading mode of global $P-E$ variability, ENSO, we begin with an assessment of how the total $P-E$ variability changes. Figure 1 shows the MEM variance of annual mean $P-E$ for the entire simulated 20^{th} Century, the projected 21^{st} Century and the difference. In this case the $P-E$ variability is contributed to by ENSO, all other large-scale modes of $P-E$

variability in the models (e.g. model representations of Atlantic variability, Indian Ocean sector variability, decadal Pacific variability, the North Atlantic Oscillation, annular modes etc.) as well as by the smaller scale and higher frequency variability often referred to as 'noise' in the climate research literature but commonly considered to be weather. There is a clear increase of interannual $P - E$ variability over the tropical Pacific Ocean where ENSO originates. That is, the difference between the positive El Niño anomalies and negative La Niña anomalies becomes larger in the 21^{st} Century as the climate warms. The percent change in total variance is shown in Figure 2a. An increase in variance occurs across almost the entire planet with maximum increases in the tropical Pacific and polar regions. There are regions of decrease over southern North America, Central America, the subtropical Atlantic Ocean, the equatorial Atlantic Ocean and northeast Brazil and over parts of the subtropical eastern Pacific Ocean. In addition there is a clear spatial structure to the change in variance with the largest increases in the equatorial Pacific Ocean and polar regions and, in general, lesser increases, or decreases, in the subtropics.

The most obvious likely cause of a general increase in $P - E$ variability is the increase in the climatological mean specific humidity which will allow even unchanged circulation anomalies to create larger moisture convergence anomalies. The fractional change in the vertically integrated lower tropospheric specific humidity is shown in Figure 2b. It increases everywhere and has generally the same spatial structure as the increase in $P - E$ variance with tropical and high latitude maxima and subtropical minima. The pattern of change in lower tropospheric water vapor is akin to that of the change in mean $P - E$ that accompanies global warning (Held and Soden 2006; Seager et al. 2010c).

However, comparing Figures 2a and 2b, it is also clear that the increase in $P - E$ variance is in some places markedly less than the change in the mean specific humidity and in others markedly greater. In work on increases in precipitation intensity it has proven possible to provide an explanation accounting only for, say, how condensation along a moist adiabat changes as the atmosphere column warms (O'Gorman and Schneider 2009) while ignoring changes in vertical velocity. This does not appear to be the case for annual mean $P - E$ variance. Figures 2c and 2d show that the variances of both the monthly mean and the annual mean vertical velocities at 700mb decline from the 20^{th} to the 21^{st} Century almost everywhere. Areas of increase are limited to the polar regions and the equatorial Pacific Ocean (and a few other isolated locations). $P - E$ is inextricably tied to the product of vertical motion and the specific humidity of the lifted air. For the widespread areas where the $P - E$ variance changes less than the increase in mean specific humidity, it is because the vertical velocity variance decreases. Consequently, for changes in the interannual variability of $P - E$, both changes in the mean specific humidity and changes in the vertical velocity variance are important. Needless to say the former is easily understood in terms of moist thermodynamics while there is less understanding of the latter because vertical motion fields are determined through a complex mix of dynamical and thermodynamical processes and across a wide range of circulation phenomena.

4. Changes in ENSO-driven interannual $P - E$ variability

We now turn our attention to that portion of the total $P - E$ variability driven by ENSO. Figure 3 shows the La Niña minus El Niño MEM mean $P - E$ pattern for the two centuries and the difference. The difference is only colored where significant at the 95% significance level using a two-sided t-test. The models show for both centuries the expected pattern with drying across the equatorial Pacific Ocean (but extending too far west compared to observations, e.g. Seager et al. (2005)) with increased $P - E$ in the Pacific Intertropical Convergence Zone (ITCZ) and South Pacific Convergence Zone (SPCZ), over the maritime continent and eastern Indian Ocean and over the tropical Atlantic Ocean and tropical South America. There is also increased $P - E$ over the Indian subcontinent and southern Asia as observed.

The change from the 20^{th} to the 21^{st} Century is an intensification of the ENSO-driven $P - E$ anomaly over the tropical Pacific, the eastern equatorial Indian Ocean, in the SPCZ and over the northern equatorial Atlantic Ocean. On the other hand the change represents a weakening of $P - E$ variability (change of opposite sign to the 20^{th} Century pattern) over the southern equatorial Atlantic Ocean, on the northern flanks of the Pacific ITCZ region and over the western equatorial Indian Ocean. Because of the much smaller subtropical and extratropical $P-E$ anomalies compared to their tropical counterparts, and because of the importance of the variability over land, the 20^{th} Century $P-E$ variability and 21^{st} minus 20^{th} Century changes are shown for Africa and Asia in Figure 4 and for North and South America in Figure 5. The changes over Africa do not represent either a systematic weakening or strengthening but are quite spatially variable. An interesting feature is the development of a coherent ENSO-driven $P-E$ anomaly over the Sahel in the 21^{st} Century that did not exist in the prior century in the models (though it does in observations (Giannini et al. 2003)). In East Africa the dry-wet north south dipole extending from Somalia to Mozambique intensifies significantly. Over central and northern India, Bangladesh and southeast Asia the ENSO-driven $P-E$ anomaly intensifies to a statistically significant amount in the 21^{st} Century.

Over North America (Figure 5) the ENSO-driven $P-E$ anomaly strengthens in southern Mexico, weakens from central Mexico to the southern U.S. and in the Pacific Northwest but strengthens in northern California and northeast North America. Although not clear in the figure, there is a modest northward extension of the region with negative $P-E$ during La Niña events. Very little of these changes over North America achieve even modest levels of statistical significance. For South America ENSO-driven $P-E$ variability weakens in northeast Brazil and strengthens in southeast South America between $20°$ and $30°S$, both differences being statistically significant at the 95% level.

a. Contribution of dynamic and thermodynamic mechanisms to changes in interannual ENSO-driven $P-E$ variability

In many parts of the world modeled $P-E$ variability intensifies as might be expected due to rising specific humidity but this is not a universal result with some areas of strong teleconnections to ENSO (e.g. southern North America and northeast Brazil) showing a weakening of interannual $P-E$ variability. Next we examine the mechanisms responsible for the modeled ENSO-driven $P-E$ variability and its change between the two centuries. Figure 6 shows the contribution of the mean circulation dynamics, δMCD term for the 20^{th} and 21^{st} Centuries and the difference. This is the term that gives rise to ENSO-driven

$P - E$ anomalies as a consequence of changes in atmospheric circulation working on the climatological humidity. Comparing to Figure 3 it is clear that the MCD term has the same global spatial pattern and amplitude as the $P - E$ variability itself, for both centuries. That is, ENSO-driven $P - E$ variability is to first order a consequence of circulation, not humidity, variability (Seager and Naik 2011), and this remains the case under climate change. In most areas the 20^{th} to 21^{st} Century change in δMCD amplifies the 20^{th} Century pattern with the exception of the western tropical Indian and equatorial Atlantic Oceans where it contributes a weakening.

Figure 7 show the contribution of the thermodynamic term, δTH, to the ENSO-driven $P - E$ variability. This term is several times smaller than the δMCD term in both centuries. In regions of mean low level divergence, such as over the equatorial Pacific cold tongue, negative specific humidity anomalies during La Niña events, and positive anomalies during El Niño events, creates a tendency to positive $P - E$ anomalies that weakly offset the δMCD contribution. An opposite sign δTH contribution is over the western equatorial Pacific where the mean low level flow is convergent.

The change from the 20^{th} to 21^{st} Century of the δTH term is extremely small (Figure 7, bottom) (although it has the same sign as its 20^{th} Century pattern as expected from rising humidity) and will be discussed no more. On the other hand the change in the pattern of ENSO-driven $P - E$ variability is almost entirely accounted for by the change in the δMCD contribution (Figure 6, bottom). That is, just as circulation variability creates the global pattern of $P - E$ variability, so it is that changes in the circulation variability contribution cause the 20^{th} to 21^{st} Century change. Of course there will be a thermodynamic contribution to the change in δMCD as unchanged circulation anomalies become more effective in a moistening atmosphere. Hence we next break down δMCD into its two constituent parts as in Eqs. 13-15.

Figure 8 shows the change in the δMCD term and contributions to this from the change in specific humidity, working with the unchanged circulation variability, and the change in circulation variability, working with the unchanged specific humidity. Reassuringly so, the term that reflects the impact of rising specific humidity simply acts to amplify the δMCD term and, hence, the $P - E$ variability. However the term that reflects the change in ENSO-driven circulation variability is in many locations as large as, or larger than, the term with the mean humidity increase. For example this term creates the north-south dipole in the change in $P - E$ variability over the tropical Atlantic and contributes significantly to the change in $P - E$ variability over the Indian Ocean. It also adds to the impact of rising humidity by increasing the strength of the negative δMCD term over the central equatorial Pacific Ocean and of the positive δMCD term over the maritime continent region. In the northern Pacific ITCZ region the change in the δMCD term is negative, which represents a weakening of the δMCD term, and this is caused by a weakening of the circulation anomaly. In contrast in the South Pacific Convergence Zone the change in the δMCD term is a strengthening of the contribution to positive $P - E$ anomalies and this is caused by a strengthening of the circulation variability.

b. *Relationship of changes in the dynamic contribution to ENSO-driven interannual $P - E$ variability to changes in vertical velocity variability*

So far we have shown that ENSO-driven $P - E$ variability is dominated by circulation variability working on the climatological specific humidity, that the 20^{th} to 21^{st} Century rise in humidity creates a tendency to more extreme $P - E$ variability but that this can be interfered with by changes in the circulation variability itself. The importance of vertical motion in determining the horizontal moisture convergence and divergence anomalies that control $P - E$ anomalies suggests that we may be able to better understand the changes in the dynamic contribution to $P - E$ variability by examining vertical velocity variability. Figure 9 shows the MEM ENSO-driven variability of the vertical pressure velocity at 700mb for the 20^{th} and 21^{st} Centuries and the difference. The vertical pressure velocity has been multiplied by minus one so that positive is upward and so that the color scale matches that for $P - E$ (green-wet-upward motion, brown-dry-downward motion). The difference is also plotted in contours on top of the 20^{th} Century values in colors (bottom panel).

During model La Niñas, relative to El Niños, there is descending motion across the equatorial Pacific Ocean with ascending motion in the ITCZ region to the north and the SPCZ region to the southwest and also over the maritime continent-eastern Indian Ocean region. There is also widespread descent in the subtropics to mid-latitudes, including over southern North America. These model patterns are quite similar to observed patterns and are related to widespread subtropical to mid-latitude drought during La Niñas (Seager et al. 2003, 2005; Seager 2007). The change in vertical velocity variability from the 20^{th} to the 21^{st} Century has some character of a reduction in amplitude, for example in the north Pacific ITCZ region and over the West Pacific warm pool and over the equatorial Atlantic Ocean. Elsewhere, increases in amplitude occur over the central equatorial Pacific Ocean, over the Atlantic at about $10°N$ and over the eastern equatorial Indian Ocean. There is also a notable weakening of the amplitude of vertical velocity variability over southern North America.

The spatial pattern of change in vertical velocity variability is very similar to that of the variable circulation contribution to the δMCD term (Figure 8, bottom) indicating that the latter is closely controlled by the former. Given the strength of the contribution of change in circulation variability to the change in $P-E$ variability, the pattern of the change in vertical velocity variability is also quite similar to the pattern of the change in the total δMCD term (Figure 6, bottom).

It has been well established that the mean tropical circulation weakens as a consequence of global warming (Vecchi and Soden 2007) which be explained in terms of energy balance constraints when specific humidity humidity rises at a faster rate than surface evaporation (Betts and Ridgway 1989; Betts 1990, 1998; Held and Soden 2006). It might be thought that these same constraints would cause ENSO-driven vertical motion anomalies to weaken. Since teleconnection patterns to higher latitudes are fundamentally driven by upper tropospheric divergent wind anomalies (Sardeshmukh and Hoskins 1988; Trenberth et al. 1998) this could then lead to weaker forced Rossby wave trains and associated circulation anomalies. This however does not appear to be generally the case. Circulation variability instead changes in a more complex manner probably related to changes in the location of ENSO SST anomalies, the basic state that impacts both the Rossby wave source and the flow through which Rossby waves propagate and the transient eddy-mean flow interaction that strongly controls the extratropical wave response to ENSO (Hoerling and Ting 1994; Seager et al. 2010b; Harnik et al. 2010).

5. Conclusions

We have investigated whether global warming leads to an increase in the amplitude of interannual $P - E$ variability. This might be expected because of the increase in water vapor content of the atmosphere which has been shown previously to cause an increase in climatological precipitation extremes with wet areas getting wetter and dry areas getting drier, a phenomenon also known as 'rich get richer' (Held and Soden 2006; Chou et al. 2009; Seager et al. 2010c). This is examined using IPCC AR4/CMIP3 simulations of the 20^{th} Century and projections of the 21^{st} Century with the A1B emissions scenario, evaluating variability over each entire century. The results are as follows:

- As expected the amplitude of total interannual $P - E$ variability increases almost everywhere across the planet. The highest increases, of 40% or more, are over the equatorial Pacific and at high latitudes. Increases of around 10% are more common elsewhere. Over the eastern subtropical Pacific Ocean, over the subtropical Atlantic $P - E$ and over southwestern North America $P - E$ variability actually weakens. This spatial pattern is somewhat akin to the pattern of climatological $P - E$ change. It is also similar to that of the change in lower tropospheric moisture content but more accentuated. In regions where the $P - E$ variance increases less than the mean specific humidity it can be explained because of a near global decrease in the amplitude of (annual and monthly mean) vertical velocity variability. Vertical velocity variance does increase over the equatorial Pacific and at polar latitudes, all regions of maximum increases in $P - E$ variance.

- In the tropical Pacific region ENSO-driven $P - E$ variance also increases from the 20^{th} to the 21^{st} Century by as much as a quarter. Elsewhere changes in ENSO-driven variance are more complex. In the Indian subcontinent, southeast Asia and Indonesia there is also an increase. Over eastern Africa the north-south dry-wet dipole during La Niñas with centers in Somalia-Ethiopia and Kenya-Mozambique strengthens. A stronger Sahel variability also develops. Over Central America ENSO-driven variance increases while over southern North America it decreases but not by a statistically significant amount. Northeast Brazil experiences a statistically significant weakening of ENSO-driven variance.

- ENSO-driven $P - E$ variance is overwhelmingly dominated by circulation anomalies working with the climatological mean specific humidity. I.e. it is 'dynamics dominated' with anomalies in the mean flow being primarily responsible. As specific humidity rises in a warmer atmosphere it would be expected that this mean circulation contribution to $P - E$ anomalies would strengthen. This is indeed the case. However the contribution from the change in the ENSO-driven circulation anomalies is just as important. It is this term that allows ENSO-driven $P - E$ variance to decrease in amplitude, such as over the equatorial Atlantic Ocean and northeast Brazil and southern North America.

- The change in the contribution of circulation variability to ENSO-driven $P-E$ variability is closely matched by the change in ENSO-driven 700mb vertical velocity variability. Over the equatorial Pacific Ocean there is an eastward shift of the longitude of maximum vertical velocity variance. This, however, does not translate into an eastward shift of the longitude of maximum $P - E$ variance because the influence of the specific humidity increase is centered west of the dateline. Over the tropical Atlantic Ocean La Niña events are associated with equatorially symmetric anomalous ascent. In the 21^{st} Century this ascent anomaly weakens south of the equator but strengthens north of the equator creating the dipole of change in ENSO-driven $P - E$ anomaly.

To summarize, on the interannual timescale the widely held belief that hydroclimate variability intensifies as a result of global warming is confirmed to be true, according to the models participating in CMIP3 and assessed by IPCC AR4. Only in a few, mostly subtropical, areas of the globe, but notably including southern North America, does the interannual variability of $P-E$ weaken. The dominant global mode of hydroclimate variability is ENSO which is also the only mode to possess proven predictability on the seasonal to interannual timescale. ENSO-driven $P - E$ variability in the models does not increase uniformly, and in some places weakens, because of changes in the ENSO-driven circulation variability. It is not understood why the total and ENSO-driven vertical velocity anomalies change in the way they do. However it is not fully understood why the observed or modeled 20^{th} Century ENSO-driven vertical motion velocities have the spatial patterns and magnitudes that they do (see Seager et al. (2005)). Hence it seems premature to explain the 20^{th} to 21^{st} Century change in vertical velocity variability. Here we just note that in considering the primary potentially predictable component of $P - E$ variability caution is in order in anticipating how it will change. Since it is caused by circulation variability, changes in intra-tropical and tropical to extratropical teleconnections can cause altered locations and amplitudes of ENSO-driven $P-E$ anomalies. However in some place, such as most of southern Asia, total hydroclimate variability, and its ENSO-driven component, do in fact strengthen from the 20^{th} to the 21^{st} Century. This is one of many regions of the world where natural variability of climate already wreaks havoc in terms of floods, droughts, crop failures, food shortages, and loss of human life. According to the model results presented here, quite apart from any change in mean climate, the variability of climate, no longer natural but a mixed hybrid of internal atmosphere-ocean variability and human-induced climate change, will only become more extreme amplifying stress on societies that are already hard pressed to cope with current day, more muted, variability.

Acknowledgments.

This work was supported by NOAA grants NA08OAR4320912 and NA10OAR4320137 and NSF grant ATM-08-04107. LV was supported as a summer undergraduate intern at Lamont by NSF grant OCE-06-49024. The comments and advice of Lisa Goddard and Arthur Greene and the Global Decadal Hydroclimate (GloDecH) group at Lamont and Columbia were essential to the progress of this work.

REFERENCES

Betts, A. K., 1990: Greenhouse warming and the tropical water vapor budget. *Bull. Amer. Meteor. Soc.*, **71**, 1464–1465.

Betts, A. K., 1998: Climate-convection feedbacks: Some further issues. *Climatic Change*, **39**, 35–38.

Betts, A. K. and W. Ridgway, 1989: Climatic equilibrium of the atmospheric convective boundary layer over a tropical ocean. *J. Atmos. Sci.*, **46**, 2621–2641.

Cattiaux, J., R. Vautard, C. Cassou, P. Yiou, V. Masson-Delmonte, and F. Codron, 2010: Winter 2010 in Europe: A cold event in a warming climate. *Geophys. Res. Lett.*, **37**, doi:10.1029/2010GL044 613.

Chou, C., J. D. Neelin, C. Chen, and J. Tu, 2009: Evaluating the 'rich-get-richer' mechanism in tropical precipitation change under global warming. *J. Climate*, **22**, 1982–2005.

Dole, R., et al., 2011: Was there a basis for anticipating the 2010 Russian heat wave? *Geophys. Res. Lett.*, **38**, doi:10.1029/2010GL046 582.

Giannini, A., R. Saravanan, and P. Chang, 2003: Oceanic forcing of Sahel rainfall on interannual to interdecadal timescales. *Science*, **302**, 1027–1030.

Groisman, P. Y., R. W. Knight, D. R. Easterling, T. R. Karl, G. C. Hegerl, and V. N. Razuvaev, 2005: Trends in intense precipitation in the climate record. *J. Climate*, **18**, 1326–1350.

Harnik, N., R. Seager, N. Naik, M. Cane, and M. Ting, 2010: The role of linear wave refraction in the transient eddy-mean flow response to tropical Pacific SST anomalies. *Quart. J. Roy.Meteor. Soc.*, 2132-2146.

Held, I. M. and B. J. Soden, 2006: Robust responses of the hydrological cycle to global warming. *J. Climate*, **19**, 5686–5699.

Hoerling, M. P. and M. Ting, 1994: Organization of extratropical transients during El Niño. *J. Climate*, **7**, 745–766.

Huang, H., R. Seager, and Y. Kushnir, 2005: The 1976/77 transition in precipitation over the Americas and the influence of tropical SST. *Clim. Dyn.*, **24**, 721–740.

Intergovernmental Panel on Climate Change, 2007: *Climate Change: The IPCC Scientific Assessment*. Cambridge University Press, Cambridge, England, 365 pp.

Meehl, G., C. Covey, T. Delworth, M. Latif, B. McAvaney, J. F. B. Mitchell, R. J. Stouffer, and K. E. Taylor, 2007: The WCRP CMIP3 multimodel dataset: A new era in climate change research. *Bull. Amer. Meteor. Soc.*, **88**, 1383–1394.

Neelin, J. D., M. Munnich, H. Su, J. E. Meyerson, and C. E. Holloway, 2006: Tropical drying trends in global warming models and observations. *Proc. Nat. Acad. Sci.*, **103**, 6110–6115.

O'Gorman, P. and T. Schneider, 2009: The physical basis for increases in precipitation extremes in simulations of 21st-century climate change. *Proc. Nat. Acad. Sci.*, **106**, 14 773–14 777.

Pall, P., T. Ainu, D. A. Stone, P. A. Stott, T. Nozawa, A. G. J. Hilberts, D. Lohmann, and M. R. Allen, 2011: Anthropogenic greenhouse gas contribution to flood risk in England and Wales in autumn 2000. *Nature*, **470**, 382–386.

Sarachik, E. S., 2011: The tools needed to provide information for adaptation to future climate conditions. *Proceedings of the 2nd International Conference: Climate, Sustainability and Development in Semi-Arid Regions, August 16 - 20, 2010, Fortaleza - Cear, Brazil*, in press.

Sardeshmukh, P. D. and B. J. Hoskins, 1988: The generation of global rotational flow by steady idealized tropical divergence. *J. Atmos. Sci.*, **45**, 1228–1251.

Seager, R., 2007: The turn-of-the-century North American drought: dynamics, global context and prior analogues. *J. Climate*, **20**, 5527–5552.

Seager, R., N. Harnik, Y. Kushnir, W. Robinson, and J. Miller, 2003: Mechanisms of hemispherically symmetric climate variability. *J. Climate*, **16**, 2960–2978.

Seager, R., N. Harnik, W. A. Robinson, Y. Kushnir, M. Ting, H. P. Huang, and J. Velez, 2005: Mechanisms of ENSO-forcing of hemispherically symmetric precipitation variability. *Quart. J. Roy. Meteor. Soc.*, **131**, 1501–1527.

Seager, R., Y. Kushnir, M. Ting, N. Naik, and J. Nakamura, 2010a: Northern hemisphere winter snow anomalies: ENSO, NAO and the winter of 2009/10. *Geophys. Res. Lett.*, **37**, doi:10.1029/2010GL043 830.

Seager, R. and N. Naik, 2011: A mechanisms-based approach to detecting recent anthropogenic hydroclimate change. *J. Climate*, submitted.

Seager, R., N. Naik, M. A. Cane, N. Harnik, M. Ting, and Y. Kushnir, 2010b: Adjustment of the atmospheric circulation to tropical Pacific SST anomalies: Variability of transient eddy propagation in the Pacific-North America sector. *Quart. J. Roy. Meterorol. Soc.*, **136**, 277–296.

Seager, R., N. Naik, and G. Vecchi, 2010c: Thermodynamic and dynamic mechanisms for large-scale changes in the hydrological cycle in response to global warming. *J. Climate*, **23**, 4651–4668.

Seager, R., et al., 2007: Model projections of an imminent transition to a more arid climate in southwestern North America. *Science*, **316**, 1181–1184.

Trenberth, K., G. W. Branstator, D. Karoly, A. Kumar, N. Lau, and C. Ropelewski, 1998: Progress during TOGA in understanding and modeling global teleconnections associated with tropical sea surface temperature. *J. Geophys. Res.*, **103**, 14 291–14 324.

Trenberth, K., A. Dai, E. M. Rasmussen, and D. B. Parsons, 2003: The changing character of precipitation. *Bull. Amer. Meteor. Soc.*, **84**, 1205–1217.

Vecchi, G. A. and B. J. Soden, 2007: Global warming and the weakening of the tropical circulation. *J. Climate*, **20**, 4316–4340.

Webster, P. J., V. E. Toma, and H.-M. Kim, 2011: Were the 2010 Pakistan floods predictable. *Geophys. Res. Lett.*, **38**, doi:10.1029/2010GL046 346.

List of Tables

TABLE 1. Models used in this study, their country of origin, the horizontal resolution of the atmosphere component and the run used in the analysis. References to these models can be found in Vecchi and Soden (2007).

	Model name	Country	Atmospheric horizontal resolution	run number 1961-2000/2046-2065
1	CGCM3.1 T47	Canada	T47	run1/run1
2	CGCM3.1 T63	Canada	T63	run1/run1
3	CNRM CM3	France	T63	run1/run1
4	CSIRO Mk3.5	Australia	T63	run1/run1
5	GFLD CM2.0	United States	$2.5^\circ \times 2^\circ$	run1/run1
6	GFLD CM2.1	United States	$2.5^\circ \times 2^\circ$	run2/run1
7	GISS AOM	United States	$4^\circ \times 3^\circ$ (C-grid)	run1/run1
8	GISS-ER	United States	$5^\circ \times 4^\circ$ (B-grid)	run1/run1
9	IAP FGOALS	China	T42	run1/run2
10	INMCM3-0	Russia	$5^\circ \times 4^\circ$	run1/run1
11	IPSL CM4A	France	$2.5^\circ \times 3.75^\circ$	run1/run1
12	MIUB ECHO-G	Germany/Korea	T30	run1/run1
13	MIROC3-2-medres	Japan	T42	run1/run1
14	MPI ECHAM5	Germany	T63	run1/run2
15	MRI CGCM2.3	Japan	T42	run1/run1

List of Figures

Change in P-E variance using 19 AR4 models

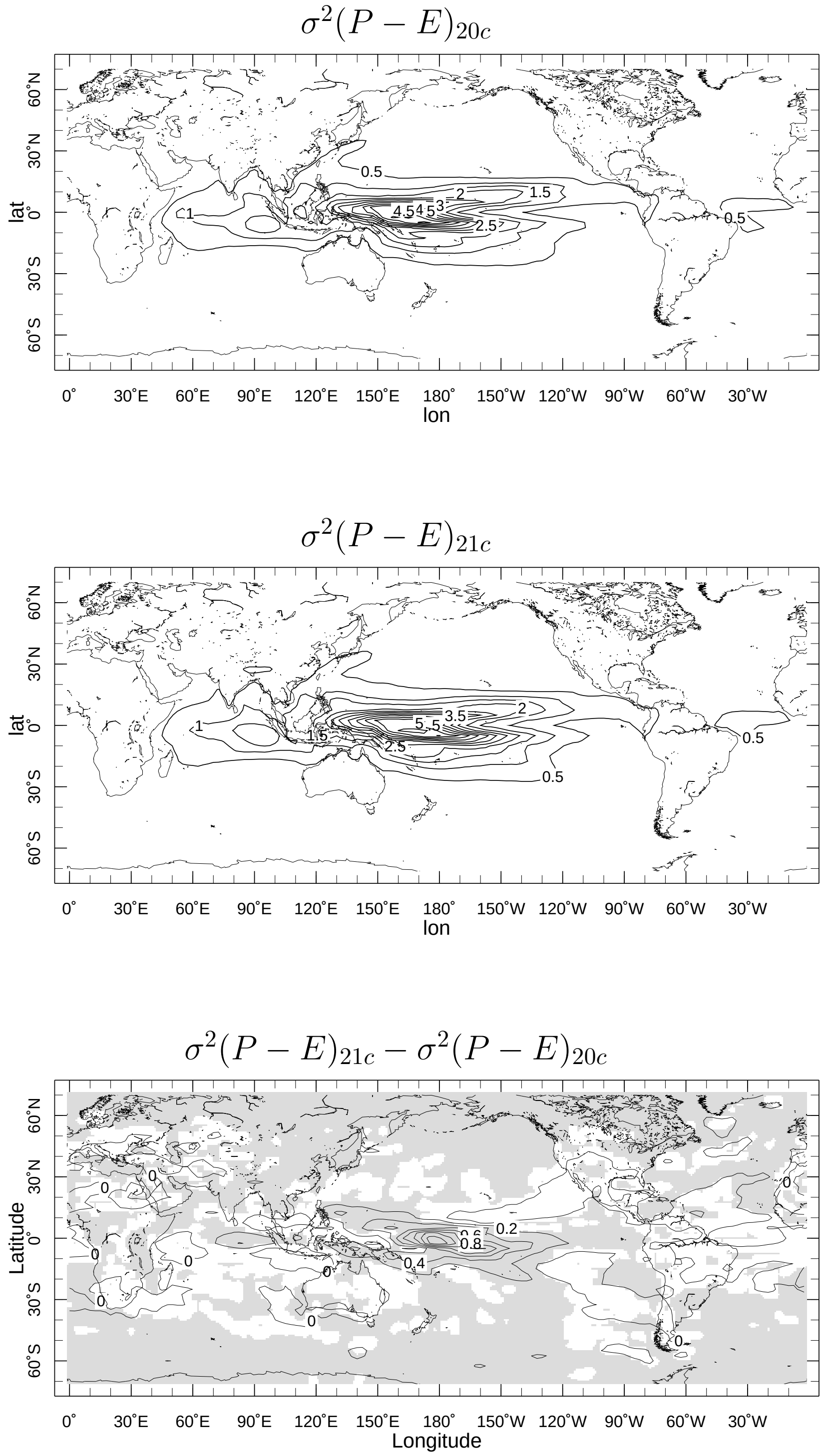

FIG. 1. The variance of annual mean $P-E$ for the 20^{th} Century (top), 21^{st} Century (middle) and the difference (bottom) evaluated for each model and then averaged across the multi-model ensemble. Shading in the lower panel indicates significance at the 95% level. Units are mm/day squared.

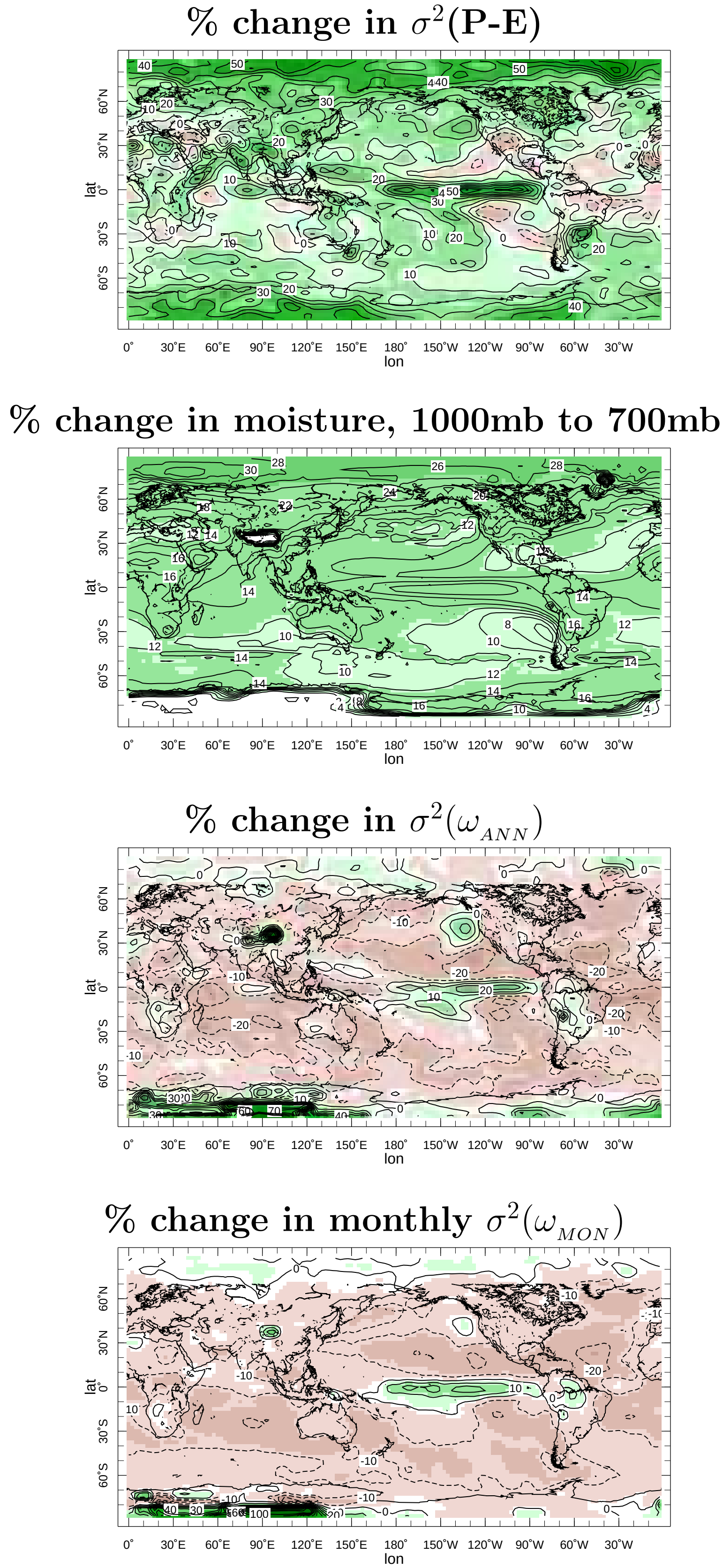

FIG. 2. The percent change in variance of the annual mean $P-E$ field (top) and the percent change in the vertically integrated specific humidity (upper middle) with the percent changes in annual mean (lower middle) and monthly mean (bottom) vertical velocity variance for the multi-model ensemble.

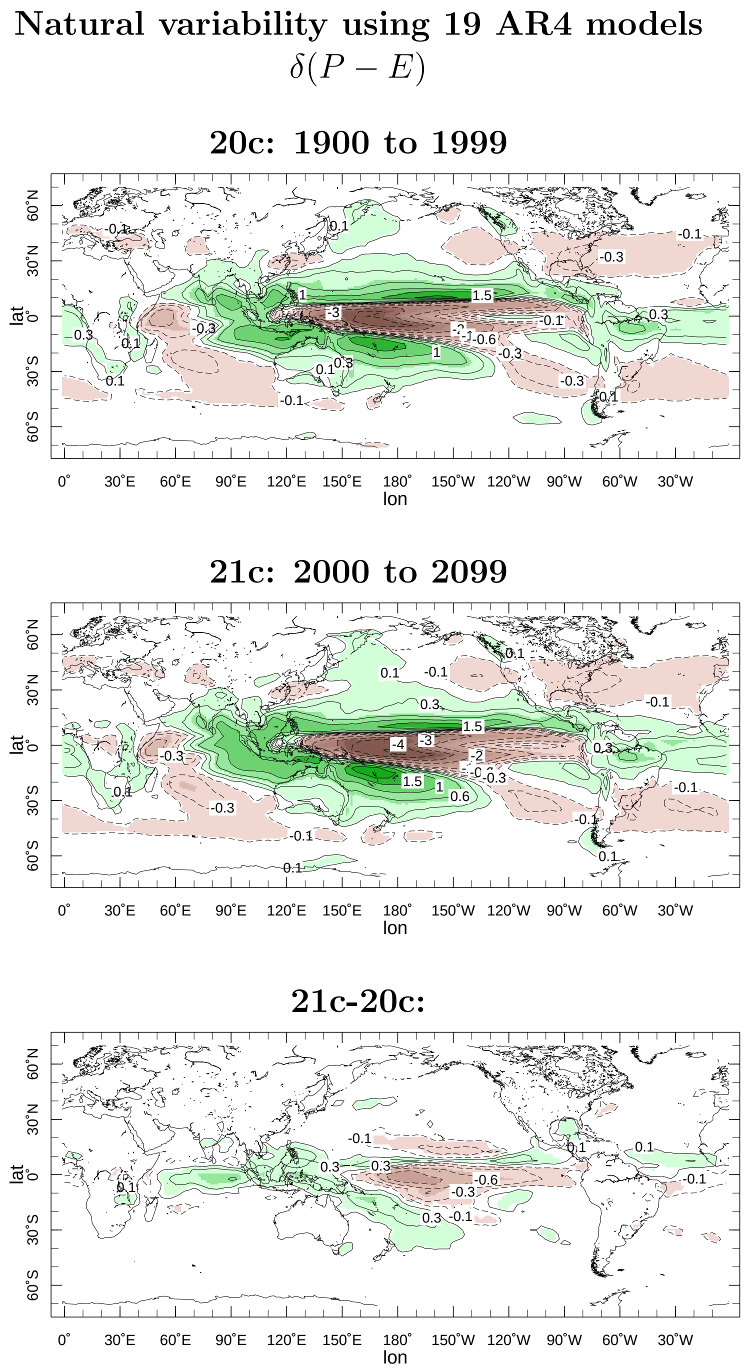

FIG. 3. The La Niña minus El Niño composite of $P-E$ (mm/day) for the multi-model ensemble for the 20^{th} Century (top), 21^{st} Century (middle) and the difference (bottom). Colors are added where the difference is significant at the 95% level.

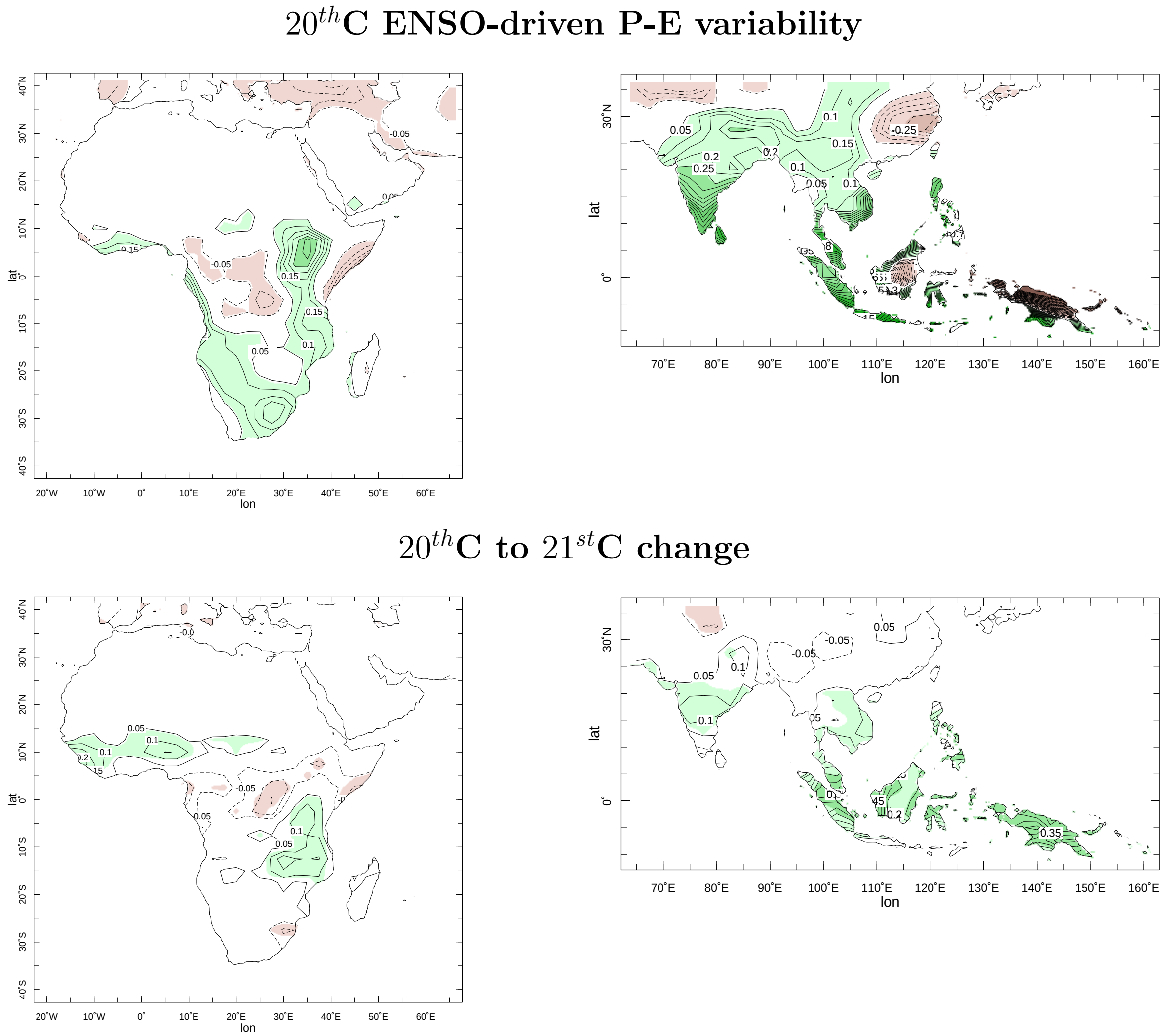

FIG. 4. As in Figure 3 but shown just for Africa and south Asia. Only regions where the difference is significant at the 95% level are colored.

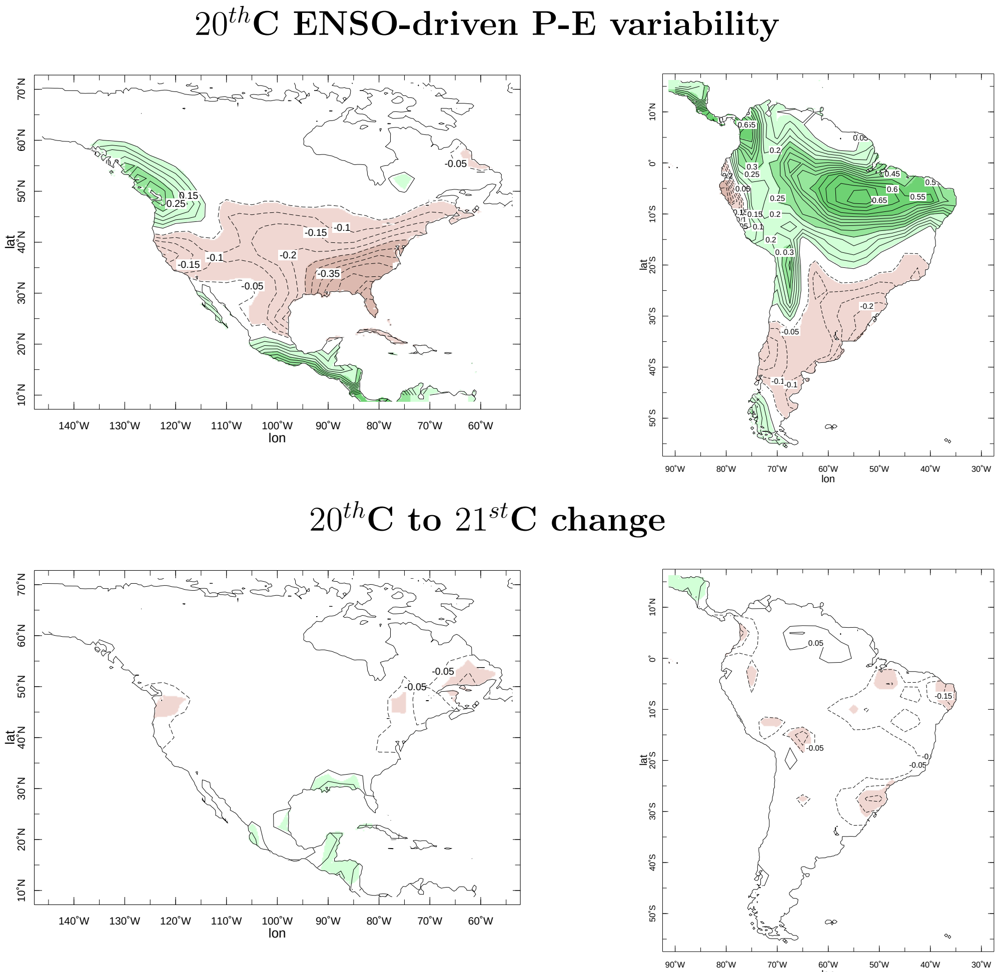

Fig. 5. As in Figure 3 but shown just for North and South America. Only regions where the difference is significant at the 95% level are colored.

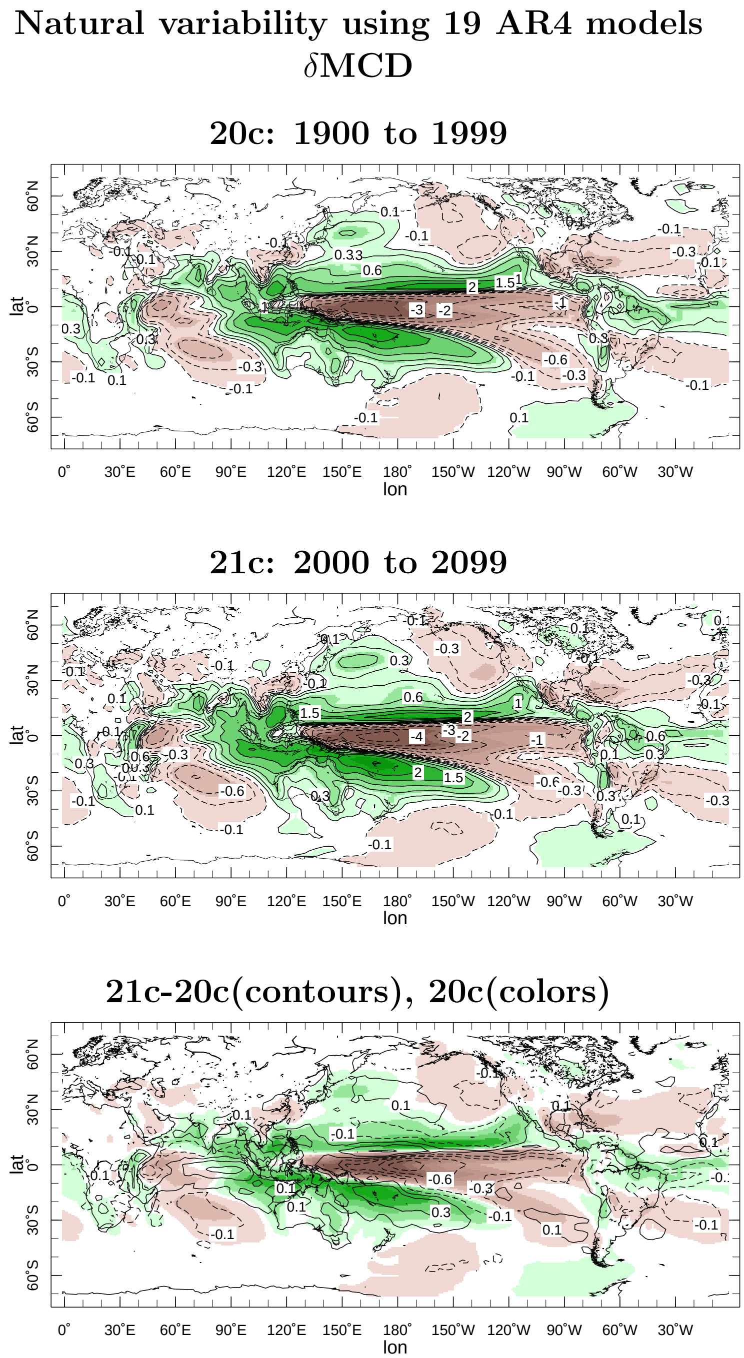

FIG. 6. The La Niña minus El Niño composite of the mean circulation dynamics (δMCD) contribution to $P - E$ variability for the multi-model ensemble for the 20^{th} Century (top), 21^{st} Century (middle) and the difference (bottom). Units are mm/day

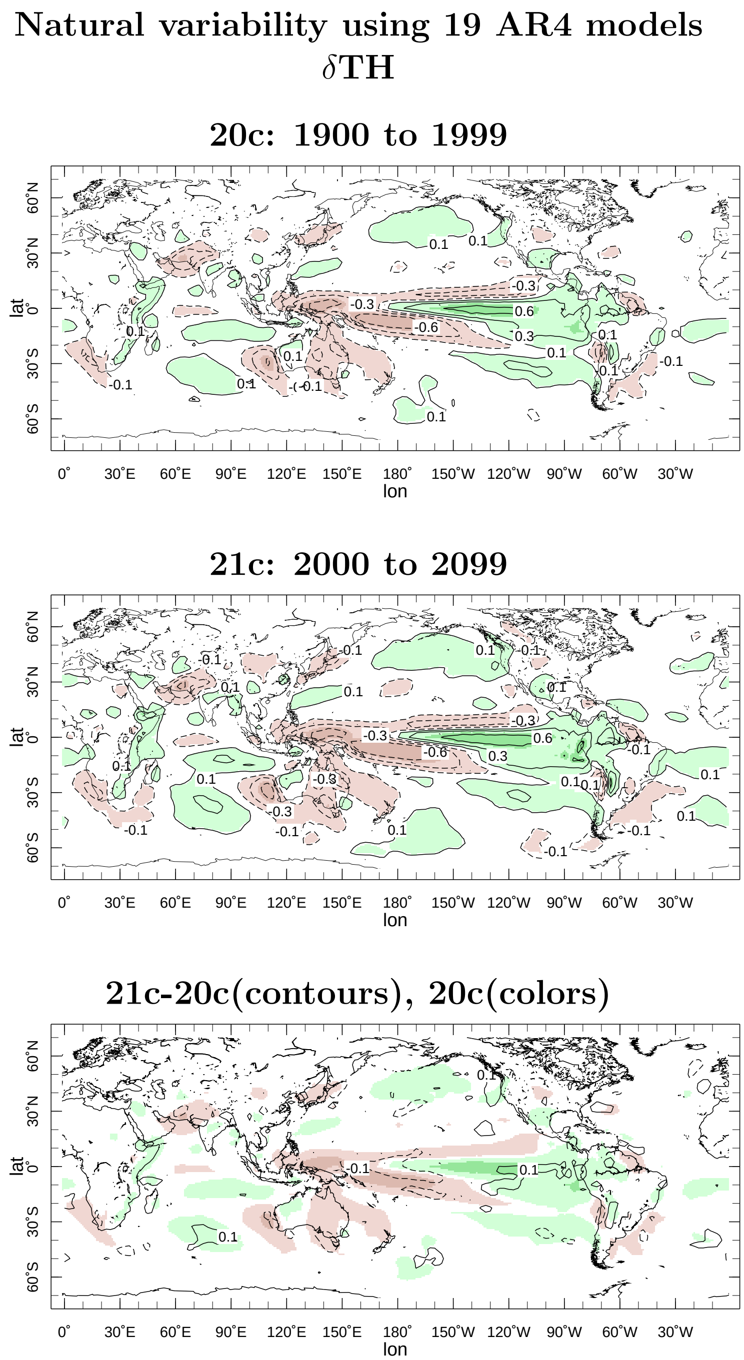

FIG. 7. Same as Figure 6 but for the thermodynamic (δTH) contribution to the La Niña minus El Niño $P - E$ composite. Units are mm/day

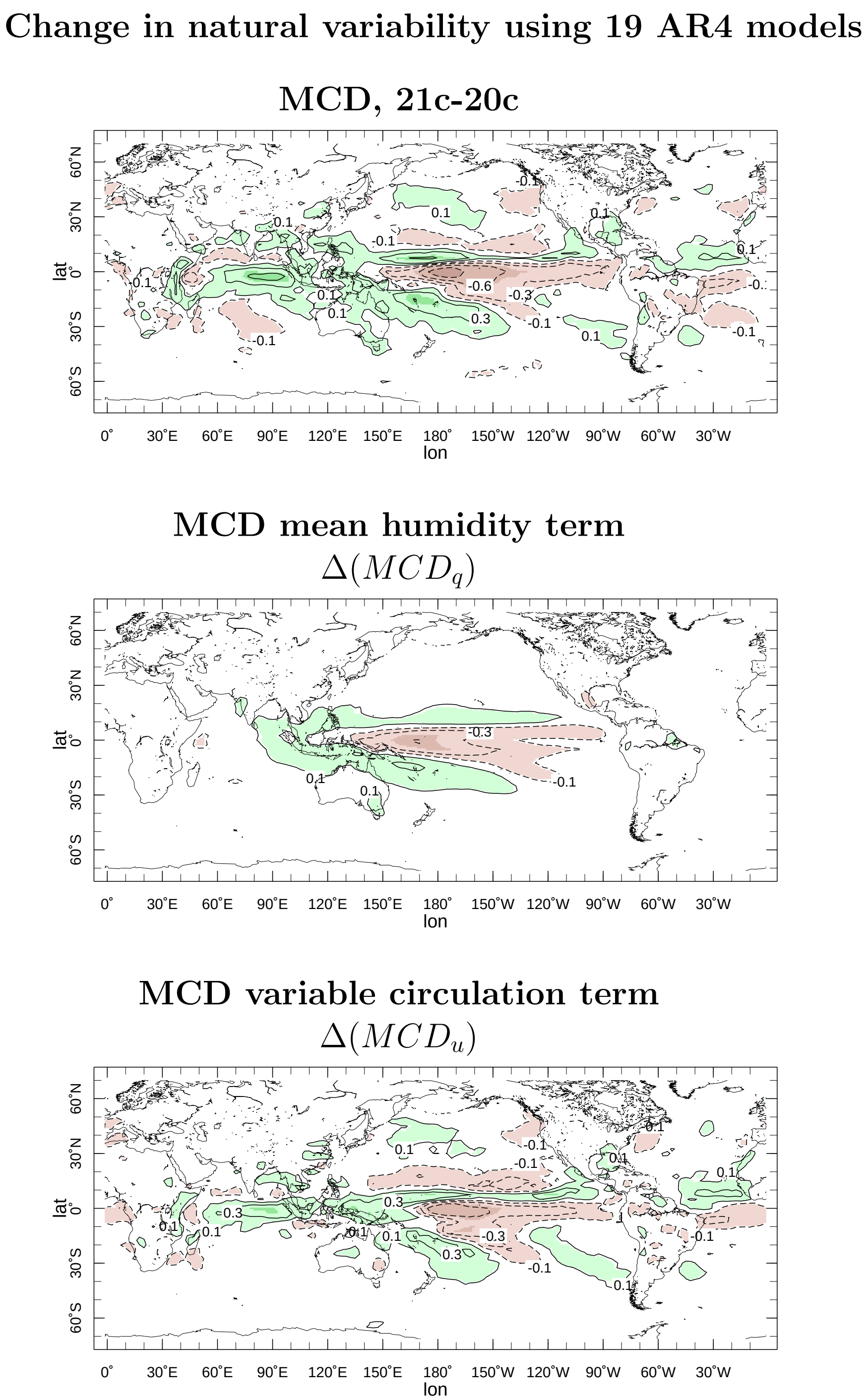

FIG. 8. The 21^{st} minus 20^{th} Century change in the La Niña minus El Niño composite of the mean circulation dynamics (δMCD) contribution to $P - E$ variability for the multi-model ensemble and the contributions to it from the change in mean specific humidity (middle) and the change in circulation variability (bottom). Units are mm/day

Change in ENSO variability of 700mb vertical velocity

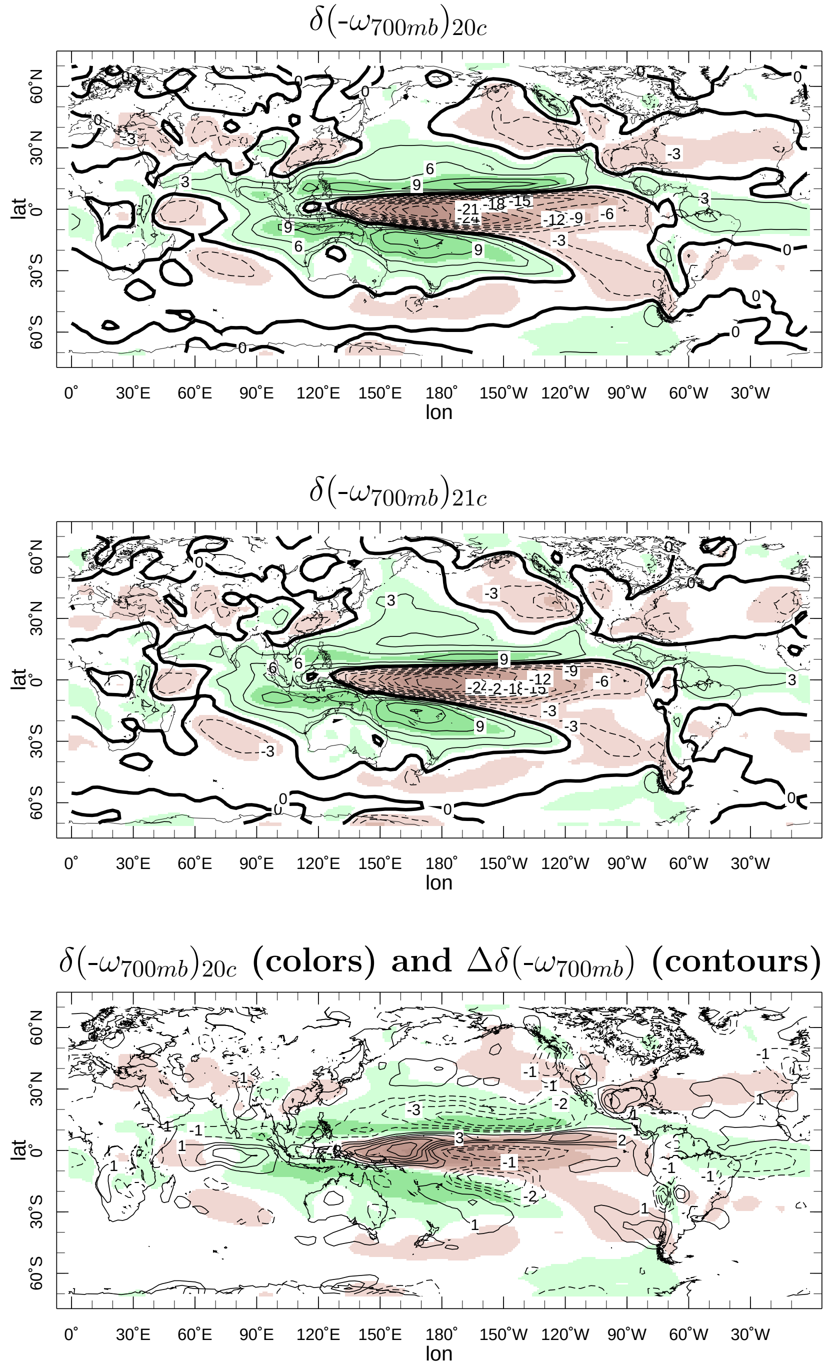

FIG. 9. The 20^{th} (top) and 21^{st} Century (middle) La Niña minus El Niño composite of the 700 mb vertical pressure velocity multiplied by minus one for the multi-model ensemble and the 21^{st} minus 20^{th} Century difference (contours) plotted on top of the 20^{th} Century values (colors) (bottom). Units are mb/day

1